Journal of Colloid and Interface Science 538 (2019) 605–610

Contents lists available at ScienceDirect

Journal of Colloid and Interface Science

journal homepage: www.elsevier.com/locate/jcis

Regular Article

Nanoparticle–nanobubble interactions: Charge inversion and re-entrant condensation of amidine latex nanoparticles driven by bulk nanobubbles

Minmin Zhang, James R.T. Seddon, Serge G. Lemay *

MESA+ Institute for Nanotechnology & Faculty of Science and Technology, University of Twente, PO Box 217, 7500 AE Enschede, the Netherlands

GRAPHICAL ABSTRACT

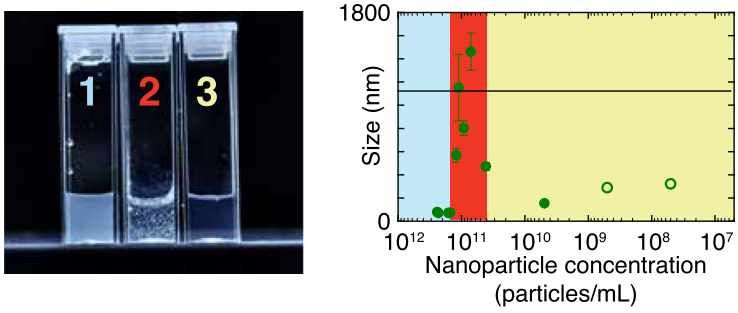

ARTICLE INFO

Article history:
Received 6 September 2018
Revised 29 November 2018
Accepted 30 November 2018
Available online 5 December 2018

Keywords:
Charge inversion
Bulk nanobubble
Positive nanoparticle
Re-entrant condensation

ABSTRACT

Hypothesis: The stability of colloidal suspensions can be influenced by supersaturation of the supporting electrolyte with gas. It has been proposed that this effect can be attributed to the formation of nanobubbles on the surface of the colloidal particles, in turn influencing DLVO forces. While previous interpretations have focused primarily on van der Waals interactions, probing positively charged particles can provide complementary insight into electrostatic interactions.

Experiments: High-power water electrolysis creates an aqueous solution supersaturated with oxygen and hydrogen. We study the ability of this solution to influence the electrophoretic properties of positive nanoparticles as a function of the particle-gas ratio. Both the ζ-potential and the effective hydrodynamic diameter of the resulting nanoentities were studied using dynamic light scattering for a range of nanoparticle sizes.

Findings: Gas-saturated solution interacts strongly with positive nanoparticles by decreasing and ultimately reversing the sign of their ζ-potential, which we attribute to the nucleation of negatively charged bubbles at the solid-liquid interface. This leads to re-entrant condensation of the particles near their point of zero charge, as directly observed via an increase in hydrodynamic diameter and macroscopic aggregation. These results indicate that modulation of electrostatic interactions can be the dominant mechanism for gas-particle interactions in these systems.

1. Introduction

Gas supersaturated solutions have attracted a lot of recent attention with the observation of stable colloids in saturated solutions following water electrolysis [1–4]. The existence of these nano-sized gas bubbles was first proposed by Parker et al. to explain the long-range (~100 nm) attractive force between two hydrophobic surfaces immersed in water [5]. Since then, evidence of both surface nanobubbles (nanoscopic gaseous bodies formed at solid/liquid interface) [1,6,7] and bulk nanobubbles (gas filled nanoscopic spherical bodies in bulk liquids) [2,6,8–11] was

* Corresponding author.
E-mail address: s.g.lemay@utwente.nl (S.G. Lemay).

https://doi.org/10.1016/j.jcis.2018.11.110
0021-9797/

reported extensively utilizing various techniques that include atomic force microscopy (AFM) [12–14], infrared spectroscopy [15],transmission electron microscopy (TEM) [16], Cryo-EM [17], and light scattering [18,19]. The general observation is that gas filled spherical particles are formed with a diameter ranging from tens to hundreds of nanometers that can survive for hours or even days in aqueous solution [2,11,20].

Much attention has been focused on nanobubbles' promise for potential applications such as wastewater treatment, mineral separation in froth flotation, ultrasound contrast agents in biomedical imaging and drug delivery in targeted chemotherapy.[9,16,21–28] However, the elucidation of the detailed mechanism for the interactions of even a simple bulk nanobubble–nanoparticle system remains incomplete [29,30].

Recently we have shown the interactions of bulk nanobubbles with negatively charged gold nanoparticles [18]. Our experiments employ high-power water electrolysis, which generates a large amount of supersaturated oxygen and hydrogen gas that can participate in bubble nucleation. This results in stable, nanobubble-like bodies with properties consistent with other reported findings [1,2] and which we therefore refer to as bulk nanobubbles here. We emphasize that our primary focus here is not on the stability mechanism, however, but rather on studying the interactions between gas supersaturated solutions and charged nanoparticles. Unlike froth flotation, where bubbles and particles interact mainly via attachment, we previously demonstrated that bulk nanobubble solutions interact with gold nanoparticles through nucleation on the gold surface, forming a new single population of particles with a diameter intermediate between those of the original nanoparticles and nanobubbles. This effect is highly dependent on the size of the gold nanoparticles, with particles sized 30 nm or less exhibiting no effect.

If our hypothesis is true that nucleation of bubbles on particles is the main mode of interaction, then interactions with positively charged particles can be expected to be significantly stronger. This is because the surface of nanobubbles, like their larger counterparts, has been shown to exhibit a negative charge [27]. Any change in net surface charge can be straightforward monitored through measuring the electrophoretic mobility of nanoparticle–nanobubble mixture solutions to extract their zeta potential.

In this work, we comparatively study the interactions of gas supersaturated solutions with both positive and negative nanoparticles employing amidine-modified polystyrene (PS) latex nanoparticles as positive nanoparticle model. We demonstrate the ability of bulk nanobubble solutions to tune the electrophoretic properties of positive nanoparticles by tuning the particle–nanobubble ratio. This effect can be so pronounced as to cause charge inversion. In a finite range of concentrations near the point of zero charge, the particles lose colloidal stability and aggregate. We believe that understanding these interactions between charged colloidal particles and charged nanobubbles can help elucidate both the phase behavior of charge stabilized colloids and proposed applications of nanobubbles such as the mechanism behind nano cleaning [31].

2. Results and discussion

2.1. Re-entrant condensation and inversion of surface charge

2.1.1. Re-entrant condensation

Electrostatic interactions are ubiquitous in polyelectrolytes, colloids and biological systems.[32–35] In mixtures of multivalent ions and macromolecules, a typical feature of phase diagrams is a phase separation regime in which macroion aggregation takes place near the isoelectric point. A subsequent restabilization and redissolution on further increasing salt concentration however takes place. This phenomenon is known as re-entrant condensation [32,33,36,37].

We now address the interactions between positively charged nanoparticles and nanobubble solutions. Fig. 1(a) is a photograph of three 100 nm amidine nanoparticle–nanobubble mixture samples at decreasing nanoparticle concentrations. Note that we do not want to overly dilute the nanobubble solution, as supersaturation would no longer be sustained. Cuvette 1 is a nanoparticle–nanobubble mixture solution with a nanoparticle concentration just above a threshold C^* where the colloids are monodisperse and stable. Cuvette 2 shows a mixture solution with nanoparticle concentration below C^*, where the positively charged latex beads aggregate. Cuvette 3 is a mixture solution with a still lower nanoparticle concentration below a second threshold C^{**}. The aggregates redissolve and the solution becomes stable and monodisperse again. Control experiments where the amidine nanoparticles are mixed with an untreated 10 mM NaCl solution do not exhibit this behavior.

This observation can be further confirmed by measuring the effective hydrodynamic diameter of the particles in mixtures, as shown in Fig. 1(c). The figure depicts a typical size evolution of 60 nm amidine latex beads mixed with gas solution at different

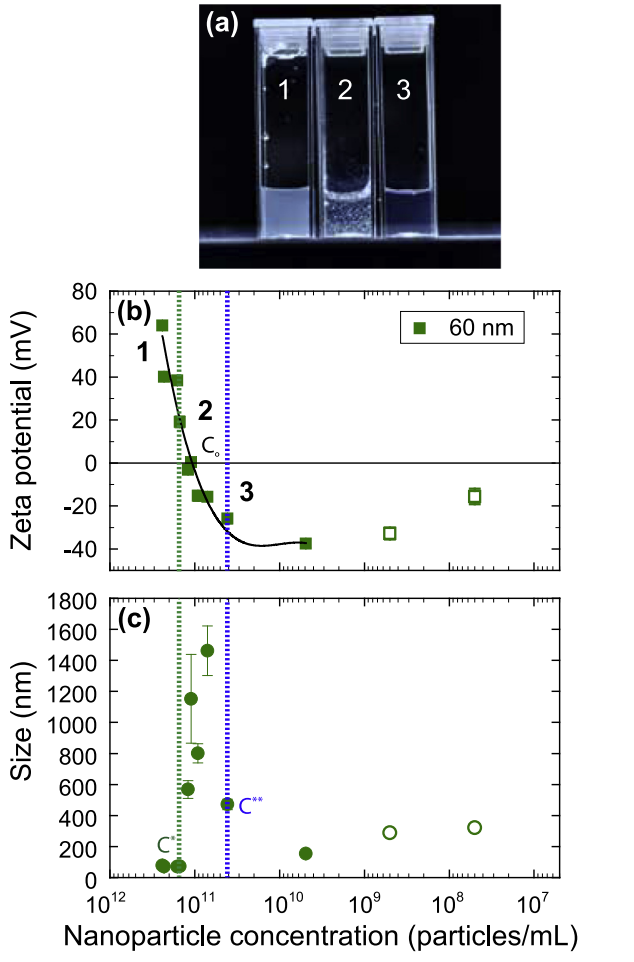

Fig. 1. (a) Photograph of 100 nm amidine latex nanoaprtice–nanobubble mixture with amidine nanoparticle concentration (1) above C^*, (2) between C^* and C^{**} and (3) after crossing C^{**}. Phase separation occurs between C^* and C^{**}. (b) Average ζ-potential and (c) apparent hydrodynamic diameter of 60 nm amidine nanoparticles and their assemblies as a function of amidine nanoparticle concentration. Note that increasing the dilution level of nanoparticles means lower nanoparticle concentration. The numbers 1,2,3 in (a) represent qualitative regions rather than specific data points in (b).

ratios. The evolution of size starts with a time- and concentration-independent average size in the range of 60–100 nm above C^*. However, after the concentration passes C^*, a dramatic increase in size occurs (~1.5 μm), which is due to the formation of amidine beads aggregates. Once the nanoparticle concentration crosses C^{**}, a sharp transition towards a smaller size, but larger than the original 60 nm nanoparticle size, is observed. This suggests that aggregates disappear and a stable colloidal suspension is restored. Upon further decreasing nanoparticle concentration, the hydrodynamic size does not vary significantly anymore, indicating that, under these conditions, the resulting nanoparticle–nanobubble nanoentities are stable against further aggregation.

2.1.2. Inversion of surface charge

Changes of the surface charge of the nanoparticles, as probed by electrophoresis and expressed as a ζ-potential, were also observed. The ζ-potential of a series of nanoparticle–nanobubble solutions as a function of nanoparticle concentration at 25 °C is presented in Fig. 1(b). At high nanoparticle concentration, the nanoparticle–nanobubble solution exhibits a positive charge. Conversely, as nanoparticle concentration decreases, the absolute value of the net charge decreases. The ζ-potential eventually crosses the point of zero charge, at which point the particles become negative. This indicates the formation of negatively charged nanoparticle–nanobubble structures, suggesting bubble nucleation on particle surfaces. This trend eventually saturates and further decreases of nanoparticle concentration do not vary the surface charge significantly. This indicates that positive particles are maximally covered by bubbles nucleated at their surfaces.

A third order polynomial fit was used to extract the point of zero charge C_o from the overall ζ-potential results. Note that the last two data points in Figs. 1(b) and (c) are plotted as open symbols. This is because once the nanoparticle concentration passes below 1×10^9 particles/mL, the DLS instrument is measuring near its sensitivity threshold. Therefore, we use only the data points before 1×10^9 for fitting the point of zero charge. Unsurprisingly, we find that the point of zero charge C_o always lays between the two phase boundaries of the phase separating regime, i.e. C^* and C^{**}, as seen by comparing Fig. 1(b) and (c).

2.1.3. Relation of charge inversion to re-entrant condensation

The evidence in Fig. 1 suggests that charge inversion represents the fundamental mechanism allowing residual attraction to cause agglomeration once electrostatic repulsion vanishes at C_o. We propose that gas nucleates at the positive particle surface, thus screening part of its overall charge and replacing it with a negative surface. Near neutrality, electrostatic interactions can no longer provide sufficient repulsion, allowing shorter ranged attractive forces to take over. This is the basic trade-off that dictates the stability of most colloids. To what extent the gas bubbles may contribute to these short-ranged interactions remains unclear.

We further systematically extended our experiments to three other different sizes of amidine nanoparticles, i.e., 20 nm, 40 nm and 100 nm. All particles show consistent aggregation and ζ-potential trends with the 60 nm particles (see supporting information for primary data). In particular, we observed re-entrant condensation for all sizes tested. The condensation boundaries C^* and C^{**} as well as the concentration at the point of zero charge were extracted for each size. A phase diagram for amidine nanoparticle solution with respect to nanoparticle diameter is shown in Fig. 2. Three regimes are recognized: regime 1 ($C > C^*$), one liquid phase exists; regime 2 ($C^* > C > C^{**}$), two phases exist; regime 3 ($C^{**} > C$), re-entrant solution, the first phase is restored.

The apparent size with respect to ζ-potential of all four nanoparticles are presented in Fig. 3. The different sizes of

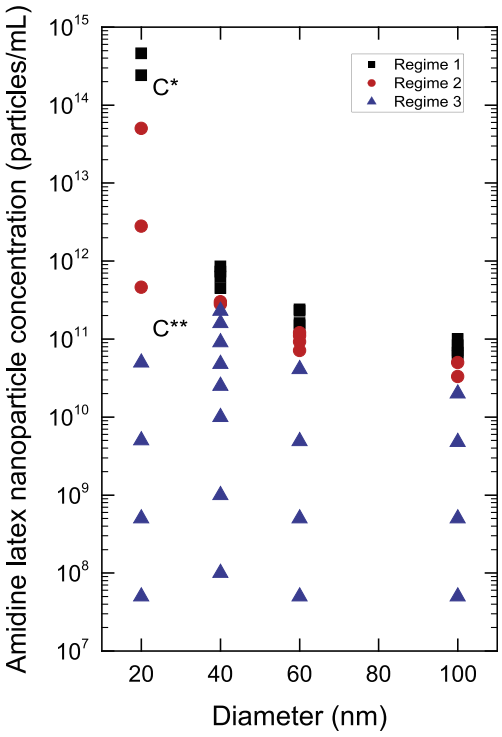

Fig. 2. Phase diagram of amidine latex nanoparticles with respect to nanoparticle sizes. The symbols represent individual samples in the respective regimes.

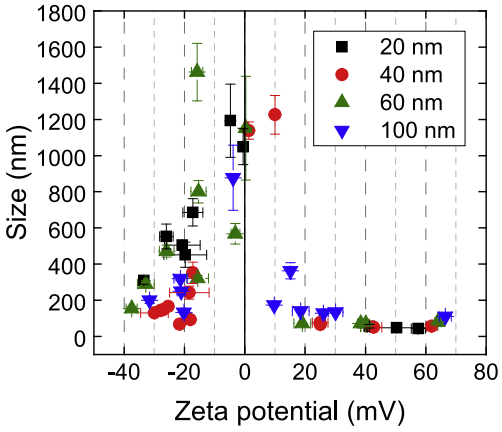

Fig. 3. Hydrodynamic diameter of amidine nanoparticles and their assemblies as a function of zeta potential with different nanoparticle sizes. The different symbols correspond to amidine nanoparticles of the following diameters: □ 20 nm, ○ 40 nm, △ 60 nm and ▽ 100 nm.

nanoparticle collapse onto a single master curve within scatter. The maximum effective diameter of the condensation product for each size is independent of the particle size under the conditions measured. This further proves that re-entrant condensation is mainly caused by charge inversion.

2.2. Influence of size of amidine nanoparticles on re-entrant condensation

2.2.1. Concentration at point of zero charge C_o

To further understand the size dependence data in Fig. 2, we extracted the nanoparticle concentration at the point of zero charge from the ζ-potential data for each particle size (third order polynomial fitting) and the resulting four data points are shown in Fig. 4.

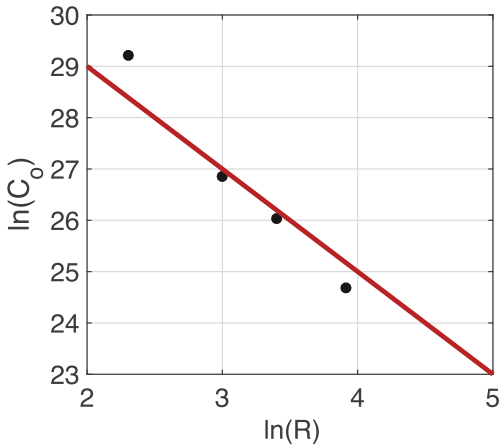

Fig. 4. Natural logarithm of nanoparticle concentration at point of zero charge with respect to nanoparticle radius. Concentration at point of zero charge of each size was estimated by a third order polynomial fitting. Four extracted concentrations were then fitted with Eq. (2), see the red curve. (For interpretation of the references to colour in this figure legend, the reader is referred to the web version of this article.)

Based on our hypothesis that reversal of surface charge of particles is due to gas nucleation at the particle surfaces, one could expect that the point of zero charge is reached when the total surface of the particles reaches a sufficiently small value to allow sufficient coverage by the available gas. The total area available per unit volume of solution, A_{tot}, is given by

$$A_{tot} = 4\pi R^2 C_o, \quad (1)$$

where C_o is the concentration of nanoparticle at the point of zero charge and R is the nanoparticle radius. To simplify analysis, Eq. (1) can be expressed as

$$\ln C_o = a - 2\ln R, \quad (2)$$

where a is the only fitting parameter. The result of a fit to this expression is shown in Fig. 4 as the red line. The good agreement suggests that the point of zero charge concentration is indeed largely driven by the available surface area under otherwise identical conditions, as indicated by Eq. (2), leading to the trend that condensation occurs at higher concentration for smaller particles.

2.3. Re-entrant condensation from a DLVO picture

The phase behavior of re-entrant condensation of amidine nanoparticle–nanobubble system can be estimated from DLVO theory [38]. This assumes that particles have to overcome an energy barrier in order to aggregate. The attractive van der Waals potential of $U_{vdW} = -AR/12d$ competes against the electrostatic double layer repulsive potential of $U_{edl} = (R/2)Ze^{-d/\lambda_D}$, where A is the Hamaker constant, R is the particle radius, λ_D is the Debye length, and $Z = 64\pi\epsilon_o\epsilon(kT/e)^2\tanh^2(e\psi_o/4kT)$ is the electrostatic interaction constant. For a monovalent 1:1 electrolyte e.g. NaCl in our system at 25 °C, $Z = 10^{-10}\tanh^2(\psi_o/103)$, where z is the electrolyte valency of 1 for NaCl, e is the unit charge of 1.6×10^{-19} C, ϵ_o is the vacuum permittivity, ϵ is the relative static permittivity of water, k is the Boltzmann constant, and ψ_o is the potential of the particle surface in mV. We use the measured zeta potential for ψ_o. The energy barrier is calculated as the maximum value (unit kT) of the sum of van der Waals attraction and electrostatic repulsion for each nanoparticle concentration.

Unfortunately, the precise Hamaker constant for our system is unknown. We plot the energy barrier of a series of 100 nm nanoparticle–nanobubble mixture solutions versus nanoparticle concentration in Fig. 5 for a typical Hamaker constant of 3.7×10^{-20} J for the air-water-air symmetrical system[39]. It is seen that the DLVO energy barrier changes in a wide range, from a very high barrier, down towards a very low barrier (close to zero), re-entrant to a relatively high barrier at low nanoparticle concentration. This behavior is qualitatively consistent with the phase changes observed in Fig. 1.

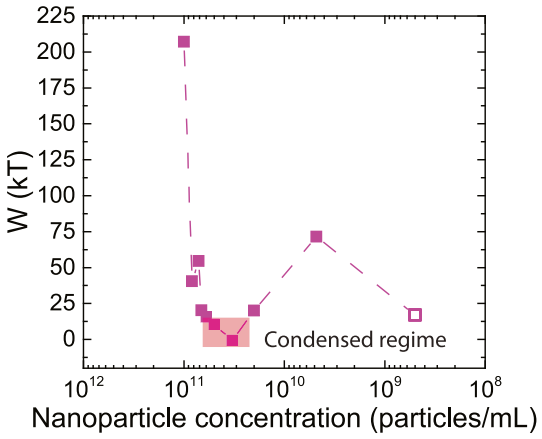

Fig. 5. Energy barriers of 100 nm amidine–nanobubble solutions calculated from DLVO theory as a function of nanoparticle concentration. The measured zeta potentials were employed as surface potentials of the nanoparticles in the calculation.

3. Conclusion

We have investigated the interactions between positively charged colloidal nanoparticles and supersaturated gas solutions. We found that gas solutions can diminish and even invert the net charge of such nanoparticles. This leads to re-entrant condensation, wherein agglomeration occurs only near the point of zero charge while the stability of the suspension is preserved at both low and high gas-nanoparticle ratios. We attribute this behavior to the formation of negatively charged nanobubbles on the surface of the nanoparticles. Our findings extend and complement earlier experiments on negatively charged particles [18], where re-entrant condensation was not observed. While those results were interpreted via a mechanism based primarily on the tuning of van der Waals forces (together with capillary forces in the case of related experiments on hydrophobic surfaces)[40–46], the present observations indicate that electrostatics can play a comparable or even dominant role in determining interparticle interactions. They also provide a new route for tuning the phase transitions of colloids initiated by bulk gas solutions, in a manner reminiscent of a series work by Drummond et al. where dissolved gas was employed to regulate surface structure [47,48]. We anticipate that this mechanism can provide a means of tuning the assembly and collective behavior of (supra) molecular systems such as cationic lipids and polypeptides.

4. Materials and methods

4.1. Nanobubble generation

Sodium chloride solutions of concentration 10 mM were prepared with milli-Q water (Millipore). The milli-Q water had a resistivity of 18.2 MΩ·cm (at 25 °C) and a TOC value below 5 ppb. The nanobubble solutions were then created by high power water electrolysis in an electrochemical flow cell. Briefly, this employs five macroscopic electrode plates made of platinum on etched titanium with a plate spacing of 2.79 mm. The salt solution was delivered at

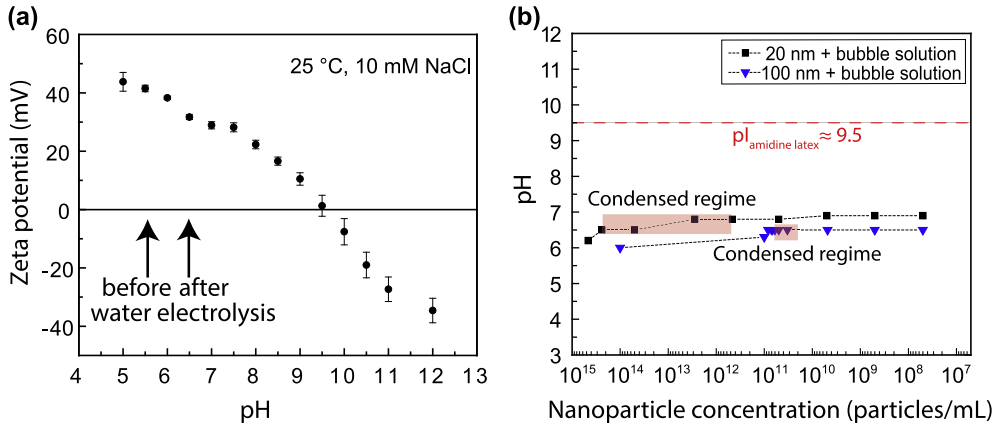

Fig. 6. (a) ζ-potential of 100 nm amidine nanoparticles as a function of pH in 10 mM NaCl at 25 °C. (b) pH measurements of nanoparticle–nanobubble solutions around phase transitions, all pH values are below the isoelectric point of amidine latex nanoparticles (9.5).

one end of the flow cell, flowed through the plates and being electrolyzed in the meantime, finally exited the flow cell downstream. During electrolysis, the aqueous solution was treated electrochemically in a two-electrode circuit configuration with a cell voltage of 24 V, an average current of 3 A, and a flow rate of 500 mL min^{-1}. The water electrolysis process splits water into oxygen and hydrogen gas, both of which dissolve back into the water stream and cause supersaturation with oxygen and hydrogen. We measured the supersaturation level of oxygen at the outlet water stream to be 110%–130% supersaturated (Fibox 3 trace 3, Fiber optic trace oxygen transmitter, PreSens). The nanobubble solution is stable on the scale of days.

4.2. Characterization of nanobubble solutions

Characterization of the nanobubble solution was carried out by dynamic light scattering (DLS, Zetasizer Nano ZS, Malvern Instruments) for sizing, electrophoresis for zeta potential (Zetasizer Nano ZS, Malvern Instruments) and nanoparticle tracking analysis (NTA, NS500, Nanosight, Malvern Instruments) for concentration, all implemented at 25 °C. Detailed experimental parameters of each technique were as follows:

DLS: The measurements were conducted in accordance with a previous publication [18]. Briefly, five measurements of 60 s duration were performed on each sample. The average and standard deviation of these measurements were used for further analysis. DLS yields particle size in terms of hydrodynamic diameter; our solutions exhibited a single-peak distribution, with peak diameter and full width at half maximum of 223 nm and 94–529 nm, respectively.

NTA: Each measurement comprised an analysis of three movies, each 60 s long and captured at a speed of 25 frames/s. The concentration was directly determined by counting the number of particles tracked in a known volume. For the solution generated by our commercial flow cell, we measured a concentration of $\sim 10^7$–10^8 particles/mL.

Electrophoresis: Three measurements were taken for each sample and each measurement took 60 s. The average and standard deviation of 3 measurements were used for further analysis. Sample holder: Folded capillary cell (DTS1061, Malvern Instruments). We measured the pristine nanobubble solution to be negatively charged with a mean zeta potential of -19 ± 3 mV.

4.3. pH of amidine latex nanoparticle solutions mixed with nanobubbles

One possible artifact is pH changes induced when mixing nanoparticle and nanobubble solutions. To exclude this possibility, we monitored the ζ-potential of 100 nm stock amidine latex nanoparticle solutions as a function of pH in 10 mM NaCl at 25 °C, as shown in Fig. 6(a). HCl and NaOH solutions were added as required to adjust pH. The particles bear positive charges originating from amidine groups, but the ζ-potential decreases as pH increases due to the protonation of amidine groups. A charge change in the ζ-potential from positive to negative occurs at high pH with an isoelectric point (pI) in the range of pH 9.0–10.0 (a linear extrapolation gives an estimate for the isoelectric point of pH 9.5.). This shows that the protonated amidine groups on the surface of the particles can be neutralized. Above the pI, the ζ-potential shows a negative sign as pH further increases which could be attributed to the hydrolysis of amidine groups, producing carboxylic groups at the surface. For comparison, the left and right arrows in the figure indicate the pH values of sodium chloride solution before and after it went through the flow cell, respectively.

As a further control, we measured the pH of a series of nanoparticle–nanobubble solutions with respect to different nanoparticle concentrations (Fig. 6(b)). It clearly shows that all the experiments described here were taking place at pH values far below the pI of amidine nanoparticles, indicating that charge inversion is not driven by changes in the pH of the mixtures.

Acknowledgement

The authors thank the Tennant Company for general financial support.

Appendix A. Supplementary material

Supplementary data associated with this article can be found, in the online version, at https://doi.org/10.1016/j.jcis.2018.11.110.

References

[1] D. Lohse, X. Zhang, Surface nanobubbles and nanodroplets, Rev. Mod. Phys. 87 (2015) 981.
[2] M. Alheshibri, J. Qian, M. Jehannin, V.S. Craig, A history of nanobubbles, Langmuir 32 (2016) 11086–11100.
[3] A.V. Postnikov, I.V. Uvarov, M.V. Lokhanin, V.B. Svetovoy, Electrically controlled cloud of bulk nanobubbles in water solutions, PLoS ONE 12 (2017) 1–18.
[4] N.F. Bunkin, A.V. Shkirin, N.V. Suyazov, V.A. Babenko, A.A. Sychev, N.V. Penkov, K.N. Belosludtsev, S.V. Gudkov, Formation and dynamics of ion-stabilized gas nanobubble phase in the bulk of aqueous nacl solutions, J. Phys. Chem. B 120 (2016) 1291–1303.
[5] J.L. Parker, P.M. Claesson, P. Attard, Bubbles, cavities, and the long-ranged attraction between hydrophobic surfaces, J. Phys. Chem. 98 (1994) 8468–8480.
[6] J.R. Seddon, D. Lohse, W.A. Ducker, V.S. Craig, A deliberation on nanobubbles at surfaces and in bulk, ChemPhysChem 13 (2012) 2179–2187.

[7] M. Hampton, A. Nguyen, Nanobubbles and the nanobubble bridging capillary force, Adv. Colloid Interface Sci. 154 (2010) 30–55.
[8] H. Kobayashi, S. Maeda, M. Kashiwa, T. Fujita, Measurements of ultrafine bubbles using different types of particle size measuring instruments, in: International Conference on Optical Particle Characterization (OPC 2014), 2014, p. 92320U.
[9] T. Temesgen, T.T. Bui, M. Han, T.-i. Kim, H. Park, Micro and nanobubble technologies as a new horizon for water-treatment techniques: a review, Adv. Colloid Interface Sci. 246 (2017) 40–51.
[10] J.H. Weijs, J.R. Seddon, D. Lohse, Diffusive shielding stabilizes bulk nanobubble clusters, ChemPhysChem 13 (2012) 2197–2204.
[11] F. Jin, J. Li, X. Ye, C. Wu, Effects of pH and ionic strength on the stability of nanobubbles in aqueous solutions of α-cyclodextrin, J. Phys. Chem. B 111 (2007) 11745–11749.
[12] C.U. Chan, L. Chen, M. Arora, C.-D. Ohl, Collapse of surface nanobubbles, Phys. Rev. Lett. 114 (2015) 114505.
[13] N. Ishida, T. Inoue, M. Miyahara, K. Higashitani, Nano bubbles on a hydrophobic surface in water observed by tapping-mode atomic force microscopy, Langmuir 16 (2000) 6377–6380.
[14] S.-T. Lou, Z.-Q. Ouyang, Y. Zhang, X.-J. Li, J. Hu, M.-Q. Li, F.-J. Yang, Nanobubbles on solid surface imaged by atomic force microscopy, J. Vac. Sci. Technol. B: Microelectron. Nanometer Struct. Process. Meas. Phenom. 18 (2000) 2573–2575.
[15] X.H. Zhang, A. Khan, W.A. Ducker, A nanoscale gas state, Phys. Rev. Lett. 98 (2007) 136101.
[16] T. Uchida, S. Oshita, M. Ohmori, T. Tsuno, K. Soejima, S. Shinozaki, Y. Take, K. Mitsuda, Transmission electron microscopic observations of nanobubbles and their capture of impurities in wastewater, Nanoscale Res. Lett. 6 (2011) 295.
[17] M. Li, L. Tonggu, X. Zhan, T.L. Mega, L. Wang, Cryo-EM visualization of nanobubbles in aqueous solutions, Langmuir 32 (2016) 11111–11115.
[18] M. Zhang, J.R. Seddon, Nanobubble-Nanoparticle Interactions in Bulk Solutions, Langmuir 32 (2016) 11280–11286.
[19] N.F. Bunkin, A.V. Shkirin, I.S. Burkhanov, L.L. Chaikov, A.K. Lomkova, Study of the nanobubble phase of aqueous NaCl solutions by dynamic light scattering, Quantum Electron. 44 (2014) 1022–1028.
[20] K. Ohgaki, N.Q. Khanh, Y. Joden, A. Tsuji, T. Nakagawa, Physicochemical approach to nanobubble solutions, Chem. Eng. Sci. 65 (2010) 1296–1300.
[21] W. Xiao, S. Ke, N. Quan, L. Zhou, J. Wang, L. Zhang, Y. Dong, W. Qin, G. Qiu, J. Hu, The role of nanobubbles in the precipitation and recovery of organic phosphine-containing in beneficiation wastewater, Langmuir 34 (21) (2018) 6217–6224.
[22] Z. Xing, J. Wang, H. Ke, B. Zhao, X. Yue, Z. Dai, J. Liu, The fabrication of novel nanobubble ultrasound contrast agent for potential tumor imaging, Nanotechnology 21 (2010) 145607.
[23] N. Rapoport, Z. Gao, A. Kennedy, Multifunctional nanoparticles for combining ultrasonic tumor imaging and targeted chemotherapy, J. Natl. Cancer Inst. 99 (2007) 1095–1106.
[24] E.Y. Lukianova-Hleb, D.S. Wagner, M.K. Brenner, D.O. Lapotko, Cell-specific transmembrane injection of molecular cargo with gold nanoparticle-generated transient plasmonic nanobubbles, Biomaterials 33 (2012) 5441–5450.
[25] S. Bhaskar, F. Tian, T. Stoeger, W. Kreyling, J.M. de la Fuente, V. Grazú, P. Borm, G. Estrada, V. Ntziachristos, D. Razansky, Multifunctional nanocarriers for diagnostics, drug delivery and targeted treatment across blood-brain barrier: perspectives on tracking and neuroimaging, Part. Fibre Toxicol. 7 (2010) 3.
[26] Y. Xing, X. Gui, Y. Cao, The hydrophobic force for bubble–particle attachment in flotation–a brief review, Phys. Chem. Chem. Phys. 19 (2017) 24421–24435.
[27] S. Calgaroto, K.Q. Wilberg, J. Rubio, On the nanobubbles interfacial properties and future applications in flotation, Miner. Eng. 60 (2014) 33–40.
[28] A. Agarwal, W.J. Ng, Y. Liu, Principle and applications of microbubble and nanobubble technology for water treatment, Chemosphere 84 (2011) 1175–1180.
[29] A.V. Nguyen, J. Nalaskowski, J.D. Miller, A study of bubble–particle interaction using atomic force microscopy, Miner. Eng. 16 (2003) 1173–1181.
[30] E.E. Meyer, K.J. Rosenberg, J. Israelachvili, Recent progress in understanding hydrophobic interactions, Proc. Nat. Acad. Sci. 103 (2006) 15739–15746.
[31] J. Zhu, H. An, M. Alheshibri, L. Liu, P.M. Terpstra, G. Liu, V.S. Craig, Cleaning with bulk nanobubbles, Langmuir 32 (2016) 11203–11211.
[32] F. Zhang, S. Weggler, M.J. Ziller, L. Ianeselli, B.S. Heck, A. Hildebrandt, O. Kohlbacher, M.W.A. Skoda, R.M.J. Jacobs, F. Schreiber, Universality of protein reentrant condensation in solution induced by multivalent metal ions, Proteins 78 (2010) 3450–3457.
[33] T.T. Nguyen, I. Rouzina, B.I. Shklovskii, Reentrant condensation of DNA induced by multivalent counterions, J. Chem. Phys. 112 (2000) 2562–2568.
[34] F. Bordi, C. Cametti, M. Diociaiuti, D. Gaudino, T. Gili, S. Sennato, Complexation of anionic polyelectrolytes with cationic liposomes: evidence of reentrant condensation and lipoplex formation, Langmuir 20 (2004) 5214–5222.
[35] B.V.R. Tata, S.S. Jena, Ordering, dynamics and phase transitions in charged colloids, Solid State Commun. 139 (2006) 562–580.
[36] A.Y. Grosberg, T.T. Nguyen, B.I. Shklovskii, Colloquium: the physics of charge inversion in chemical and biological systems, Rev. Mod. Phys. 74 (2002) 329–345.
[37] F. Roosen-Runge, B.S. Heck, F. Zhang, O. Kohlbacher, F. Schreiber, Interplay of pH and binding of multivalent metal ions: charge inversion and reentrant condensation in protein solutions, J. Phys. Chem. B 117 (2013) 5777–5787.
[38] J. Lyklema, Fundamentals of Interface and Colloid Science: Soft Colloids, vol. 5, Elsevier, 2005.
[39] J.N. Israelachvili, Intermolecular and Surface Forces, third ed., Academic Press, San Diego, 2011. pp. 266.
[40] D.R.E. Snoswell, J. Duan, D. Fornasiero, J. Ralston, Colloid stability and the influence of dissolved gas, J. Phys. Chem. B 107 (2003) 2986–2994.
[41] N. Mishchuk, J. Ralston, D. Fornasiero, Influence of dissolved gas on van der waals forces between bubbles and particles, J. Phys. Chem. A 106 (2002) 689–696.
[42] E.E. Meyer, Q. Lin, J.N. Israelachvili, Effects of dissolved gas on the hydrophobic attraction between surfactant-coated surfaces, Langmuir 21 (2005) 256–259.
[43] A. Faghihnejad, H. Zeng, Hydrophobic interactions between polymer surfaces: using polystyrene as a model system, Soft Matter 8 (2012) 2746.
[44] N. Mishchuk, J. Ralston, D. Fornasiero, Influence of very small bubbles on particle/bubble heterocoagulation, J. Colloid Interface Sci. 301 (2006) 168–175.
[45] M. Dudek, K. Muijlwijk, K. Schroën, G. Øye, The effect of dissolved gas on coalescence of oil drops studied with microfluidics, J. Colloid Interface Sci. 528 (2018) 166–173.
[46] P. Knuepfer, L. Ditscherlein, U.A. Peuker, Nanobubble enhanced agglomeration of hydrophobic powders, Colloids Surf. A 530 (2017) 117–123.
[47] G. Bepete, E. Anglaret, L. Ortolani, V. Morandi, K. Huang, A. Pénicaud, C. Drummond, Surfactant-free single-layer graphene in water, Nature Chem. 9 (2017) 347–352.
[48] I. Siretanu, J.P. Chapel, C. Drummond, Water–ions induced nanostructuration of hydrophobic polymer surfaces, ACS Nano 5 (2011) 2939–2947.